Determining the free alkali metal content in concrete – Case study of an ASR-affected dam

Plusquellec, G., Geiker, M. R., Lindgård, J., & De Weerdt, K.

Citation for the published version (APA 6th)
Plusquellec, G., Geiker, M. R., Lindgård, J., & De Weerdt, K. (2018). Determining the free alkali metal content in concrete – Case study of an ASR-affected dam. Cement and Concrete Research, 105, 111-125. doi:https://doi.org/10.1016/j.cemconres.2018.01.003

Title

Determining the free alkali metal content in concrete – case study of an ASR-affected dam

Authors

Plusquellec G.[1], Geiker M.R.[1], Lindgård J.[2], De Weerdt K.[1]

Affiliations

1: Department of Structural Engineering, Norwegian University of Science and Technology (NTNU), 7491 Trondheim, Norway

2: SINTEF Building and Infrastructure, 7465 Trondheim, Norway

Corresponding author

Plusquellec G.: gilles.plusquellec@ntnu.no

Abstract

In concrete affected by alkali–silica reaction (ASR), aggregates react in the high pH environment and cause deleterious expansion and cracking of the concrete. Leaching of alkali metals from the concrete might therefore locally reduce ASR. However, few data on alkali metals leaching are available in the literature. Our goal was to document the alkali metal leaching and to build-up an alkali inventory (the amount in solid and in solution, and the amount released by the aggregates) in a full-scale structure, the 50-year-old Votna I dam in Norway. Free alkali metal profiles were determined on cores taken at four locations with different exposure conditions: permanently immersed, periodically immersed, exposed to rain, or sheltered. Alkali leaching was observed at all four locations up to a depth of 100 mm. The leached zone exhibited less intense cracking than the non-leached concrete, indicating that the alkali leaching might be limiting ASR.

Keywords

Alkali–Aggregate Reaction (C), pH (A), alkalis (D), pore solution (B), leaching, micro-XRF

1. Introduction

Alkali–Silica Reaction (ASR) is one of the major deterioration mechanisms for concrete. Three conditions need to be fulfilled for ASR to take place: i) the presence of reactive aggregates, ii) a high pH in the pore solution, and iii) a high moisture content, i.e. above 80% relative humidity [1, 2]. If all three conditions are met, an expansive silica-rich gel can form which can lead to concrete expansion and cracking.

The pH of the pore solution of concrete typically ranges between 12.5 and 14 [3-5]. The pH is buffered up to at least 12.5 because the pore solution is saturated with respect to portlandite ($Ca(OH)_2$). The presence in the pore solution of alkali metal ions such as Na^+ and K^+ raises the pH above 12.5. The alkali metal ions are critical for the high pH levels required for ASR to take place. The pH required depends on the type and reactivity of aggregate [6]. This is reflected in the regulations that limit the alkali metal levels in concrete made with potentially reactive aggregates [7].

The alkali metals (Na and K) in the pore solution originate primarily from the constituents of the concrete – mainly from the cement, but release from the aggregates has also been reported [8, 9]. Alkali metal ions can also come from additives and external sources, such as seawater and de-icing salts, which penetrate the concrete. However, this ingress of Na^+ and K^+ is limited compared to Cl^- [10, 11]. Yet, alkali metal ions can also exit the concrete by leaching to the exterior.

This study focuses on alkali metal leaching from concrete, which has been extensively investigated in laboratory samples. Leaching of up to 100% of the total alkali metal content has been observed for submerged concrete prisms [12] and of 10–35% from samples stored above water for one year [12, 13]. The extent of leaching depends on: the storage conditions [12, 14], the specimen size [12, 15], the initial

alkali metal content [12, 16], and the binder type [12, 13]. It has been demonstrated that alkali metal leaching from concrete prisms leads to reduced expansion during ASR performance testing [12, 14, 17].

There have, however, been very few studies on alkali metal leaching in real structures [18-20]. One reason is that it is difficult to extract pore water from old concrete by expression under pressure. Grattan-Bellew and Danay [18] and Bérubé et al. [19] investigated Canadian dams that were 50 to 75 years old. They measured the free alkali metal content of concrete cores using an alternative method to extraction under pressure: the hot water extraction method. This is a leaching method where the samples are pulverized, mixed with boiling deionized water for 10 min, and cooled overnight. In these studies, however, it was not possible to determine detailed alkali metal profiles, due to either a large sample size or a large spacing between the samples. Moreover, the exposure conditions were not clearly specified. It is therefore difficult to draw conclusions about the impact of the exposure conditions on the alkali metal leaching. Kagimoto et al. [20] succeeded in extracting pore solution at high pressure from concrete cores taken from a 14-year-old dam. The pore solution near the surface (in this case, the first 100 mm) exhibited a lower alkali metal concentration than at greater depth in the concrete. Again, the exposure conditions were not clearly stated, which limits any potential generalisation of the results.

This paper presents an investigation of the influence of the environmental exposure conditions on the alkali metal leaching from the ASR-affected concrete dam, Votna I, situated in south-western Norway. Four 500–700 mm long cores were extracted from selected locations. We applied the cold water extraction method (CWE), which is a rapid leaching method [5], on 10 mm thick slices to determine the free alkali metal profiles in the concrete. Those cores go through the entire length of the structure in order to investigate the external and internal conditions of the dam. In addition, potassium profiles were determined using a micro-XRF. Thermogravimetric analysis was applied to investigate the variations in the

cement paste-to-aggregate ratio in the 10 mm slices. On four parallel cores, 50 mm slices were split off to determine water content, degree of capillary saturation, and relative humidity profiles. The water content was used to calculate the pH of the pore solution based on the free alkali metal content. Furthermore, cracking density profiles were determined on additional four parallel concrete cores using image analysis on fluorescence-impregnated plane-polished sections. The leached outer zone, with a depth of up to 100 mm in the permanently submerged core, exhibited less extensive cracking than the non-leached zone. Finally, the release of alkali metals from the aggregates to the concrete was evaluated based on the CWE results.

2. Materials and methods

2.1. The Votna I Dam

Four concrete dams were constructed between 1964 and 1966 in the Votna area of Norway. This study focuses solely on the dam called Votna I. It is a double-curved arch dam connected to a slab dam via an abutment wall (Figure 1 and Figure 2). The dam's total length is 185 m and its maximum height is 55 m. The thickness of the arch dam is 4 m at the bottom decreasing to 0.95 m at the top. The slab dam has a thickness of 0.7 – 0.8 m at the bottom and 0.3 m at the top. This study focused on the slab dam. The water level in the reservoir reaches the top of the dam during summer/autumn and is gradually lowered during winter/spring. The composition of the water in the reservoir is given in Table 1 (data retrieved in February 2017).

The concrete mix-design used for the slab dam is given in Table 2. The composition can slightly differ from one location to another. No data has been found for the concrete used in the pillars. According to the owner, Hydro Energy AS, a lower quality concrete with a lower cement content was used for the pillars.

This was confirmed in an earlier study on the Votna II slab dam cast in the same period [21]. The sand used was a granite gneiss from Nesflaten, Norway, and the coarse aggregate was a local cataclastic crushed rock. It is the coarse aggregate which is classified as potentially ASR reactive [22]. The coarse aggregate was extracted from the concrete using the method described in the section 2.2 and was analysed by XRF, using a Bruker S8 Tiger, 4 kW X-ray spectrometer. The composition of the coarse aggregate is given in Table 1. No documentation is available on the cement, but considering the period of construction, i.e. 1964–1966, a pure CEM I is thought to have been used. The statistics from the Norwegian Norcem Dalen cement factory indicate that the alkali metal content in the CEM I cement of that period was between 1.19% and 1.28% [23].

The first indications of ASR in the dam were observed in the years 1987–1988, with typical map cracking in the arch dam coupled with deformations at the top. Votna I has been investigated several times since then, with regular deformation measurements, safety evaluations and laboratory investigations of drilled cores for moisture measurement, “Crack Index” determination, gel observation, and the testing of mechanical properties. The results of these studies have been presented [21, 24], but the free alkali metal content of the concrete has never been investigated. Larsen et al. [21] confirmed that ASR was the cause of the damage observed and concluded that the reaction was still in an early stage. The deformation caused high stress concentrations in the structure at the connection point between the arch dam, the slab dam, and the abutment wall (Figure 1). Repair works were undertaken during the summer of 2015 by cutting out part of the slab dam and the abutment wall over their entire height (about 15–16 m) to release the compressive stresses: about 1 m width for the slab dam and about 0.5 m width for the abutment wall (Figure 3-f). These repairs meant that the water reservoir had to be completely emptied, which gave a unique opportunity to drill concrete cores from locations usually not accessible.

The structure was inspected in May 2015. Figure 3-a and 3-b show the typical ASR map cracking, Figure 3-c shows the presence of gel, and Figure 3-d illustrates the highly humid atmosphere inside parts of the slab dam structure. Aggregates are visible on the usually submerged surface of the concrete of the slab dam (Figure 3-e). The locations for the drilling of the cores were decided during the inspection of May 2015 (Figure 3-f). Each location corresponds to a different exposure condition, and therefore we expect a difference in alkali leaching, which can influence the extent of ASR. Figure 1 shows the various drilling locations, called W, WA, A, S and E. Location W corresponds to the bottom part of the slab dam, normally submerged in water. Location WA is in the top part of the slab dam, which is either submerged in water or exposed to atmospheric conditions (e.g. rain, snow, ice, sun) depending on the level of the reservoir. Location A corresponds to the "outside" pillar of the slab (located outside the frost wall) and is therefore only exposed to atmospheric conditions. The cores from location S were taken from the "inside" pillar (located inside the frost wall), which is sheltered from rain. Large blocks from the cut part of the slab dam (location E) were drilled for samples used for extracting the aggregates. The drilling was carried out in June 2015, and several cores were taken at each location (Figure 3-f). Each core was immediately wiped off, wrapped in plastic, and then sent to the SINTEF laboratory, where they were kept six months in a cold room (5 °C) until analysis. Only the moisture measurements were carried out on arrival at the laboratory. Table 3 gives an overview of the various samples drilled from the Votna I dam that were investigated in this study. A colour is associated with each core: dark blue for W, light blue for WA, green for A and orange for S.

The surfaces of each core are defined as "external" or "internal". "External" refers to a surface exposed to the external environmental conditions, and "internal" refers to a surface exposed to the internal conditions inside the dam (between the slab and the frost wall). The cores from locations W and WA have one "internal" surface and one "external" surface, the core from location A has two "external" surfaces,

and the core from location S has two “internal” surfaces. For the two latter cores, the surfaces are differentiated by their orientation, i.e. north or south. The left-hand side of all the graphs, sketches and pictures presented in this article corresponds to the “reference” surfaces: the “external” surfaces of the cores from locations W and WA and the north surface of the cores from locations A and S.

2.2. Methods

Separation of aggregates

The coarse aggregates were separated from the cement paste using the method presented by Haugen et al. [25]. Four samples of approx. 100 x 100 x 100 mm were cut from the large concrete blocks (location E). The samples were immersed in water for 3 days to saturate the larger pores with water. After that period, they were put in a bucket filled with liquid nitrogen until all the nitrogen had evaporated. Finally, the samples were heated in a microwave oven for 7 min at maximum power. These severe freeze/thaw cycles were applied three times to the four samples to crack them and make it possible to separate the aggregates from the paste by hammering. The aggregates were washed in a diluted HCl solution to remove the remaining cement paste and subsequently rinsed with deionized water.

Sawing/grinding

Sawing was performed with a diamond blade (thickness 2 mm) using a minimum of cooling water to avoid alkali leaching. The cores taken from locations W and WA (diameter 150 mm) were first cut lengthwise in half. The cores from locations A and S were not cut lengthwise because their diameter was smaller (90 mm). We needed sample sizes large enough to have a paste-to-aggregate ratio representative of the concrete. The half cores from locations W and WA, and the whole cores from locations A and S were cut into 10 mm thick slices. Table 3 shows the position of each slice.

Each slice was then crushed with a jaw crusher. The pieces were collected in labelled plastic bags and stored in desiccators containing soda lime prior to further treatment. CWE requires the use of fine powder (< 80 µm), so all the samples (both concrete and aggregate) were ground with a vibratory disc mill (RS200 from Retsch) at 1500 rpm for 30 seconds for the aggregate samples and 60 seconds for the concrete samples. The size of the particles was checked with an 80 µm sieve. The powders were stored in desiccators with soda lime until further analysis.

Moisture state

The moisture state of concrete can be expressed as water content (W), degree of capillary saturation (DCS), or relative humidity (RH). W gives the mass % (of concrete dried at 105 °C) of water or pore solution present in the concrete. This is then used to calculate the concentration of ions in the pore solution of the concrete samples. DCS relates to the percentage of gel and capillary pores in concrete that are filled, and is therefore independent of the paste-to-aggregate ratio of the sample. RH is often the only measure of the moisture state of the concrete used in connection with ASR, but RH describes the thermodynamic state of the pore water at a certain temperature and is not a measure of the amount of water. At a given moisture content (for example expressed as W = mass % water), the RH is a function of the pore structure (i.e. water-to-cement ratio, w/c), the temperature, the chemical composition of the pore water and the moisture history of the concrete. The relationship between the RH and the W is given as absorption/desorption isotherms.

In this study, separate cores (diameter 90 mm) were drilled. The moisture content and DCS measurements (see Table 3) were carried out using the method described by Sellevold and Farstad [26]. Each core was split into disks of approx. 50 mm thick. Each disc was then split into four pieces and brushed to remove loose particles. The four pieces of each disc were weighed together 1) just after splitting (m_{ini}), 2) after

immersion in water for 7 days (m_{water}), and 3) after drying for 7 days at 105 °C (m_{dry}). The amount of pore solution or water content (W), and the degree of capillary saturation (DCS) were calculated using Equations (1) and (2):

$$W = \frac{m_{ini} - m_{dry}}{m_{dry}} \cdot 100 \quad (1)$$

$$DCS = \frac{m_{ini} - m_{dry}}{m_{water} - m_{dry}} \cdot 100 \quad (2)$$

DCS is relatively easy to measure accurately and is regarded as a reliable method to determine the percentage of water filling the gel and capillary pores [26]. In [27], a low spread was documented for 8 parallel test series, as a mean coefficient of variance of about 1% was obtained.

In addition, selected concrete pieces split from the disks from each core (see above) were used to measure relative humidity (RH) following the procedure described by Lindgård et al. [27]:

- Each piece of concrete was split into smaller pieces, before crushing these pieces with a hammer. To avoid any influence from the water used during the drilling operation, cement mortar particles from the outer 10–15 mm of the concrete cores were not used. Throughout the crushing and sampling procedure, care was taken to avoid loss of moisture.
- The pieces of crushed cement mortar (some being stuck to small aggregate particles) with a diameter of about 4–8 mm were collected and put into glass tubes (length 150 mm, inner diameter 18 mm) until about ¾ of the glass tube was filled. The top of the glass tube was then immediately sealed with a rubber stopper and parafilm.
- A Vaisala sensor was installed in each glass tube and the glass tubes were put in an insulated box in a conditioning room (temperature 20 °C and 50% RH). Each sensor was calibrated before and after each measurement. The reported accuracy of the Vaisala sensors of type “HMP44” is ± 2% RH in the range

of 0–90% RH and ± 3% RH in the range of 90–100% RH [28]. In [27], based on parallel measurements, the spread in the RH results was low and well within the reported accuracy of the sensors.

- Daily RH readings were taken over 4–5 days. The readings taken after 2–4 days (when they had stabilised) are presented in this paper.

Thermogravimetric analysis (TGA)

Thermogravimetric analysis (TGA) was used to determine the paste/aggregate ratio in the different slices. This is important when evaluating the CWE results. A TGA/DSC 3+ from Mettler Toledo was used. Approx. 300 mg of powder per slice was poured into a 600 µl alumina crucible. This amount was representative of the corresponding slice because of the homogenization resulting from the fine grinding. The weight was monitored while the powder was heated from 40 °C to 900 °C at 10 °C/min, and the sample chamber was purged with N_2 at 50 ml/min in accordance with the guidelines from Scrivener et al. [29].

The amounts of hydrate water (H), portlandite (CH), and mass loss due to decomposition of carbonates ($\underline{C}$) as percentages of the dry mass (i.e. the mass of the dry and decarbonated sample at 800 °C) calculated as follows (Equations (3), (4) and (5)). The temperature boundaries indicated here are only informative – the exact values were determined from the derivative curves.

$$H = \frac{m_{105} - m_{550}}{m_{800}} \tag{3}$$

$$CH = \frac{m_{450} - m_{550}}{m_{800}} \cdot \frac{M(Ca(OH)_2)}{M(H_2O)} \tag{4}$$

$$\underline{C} = \frac{m_{550} - m_{800}}{m_{800}} \tag{5}$$

The amount of portlandite can be calculated from the water loss using the molar mass of portlandite, $M(Ca(OH)_2)$, 74 g/mol, and the molar mass of water, $M(H_2O)$, 18 g/mol.

The cement content (C) can be estimated from the portlandite content by assuming that 100 g of ordinary Portland cement with a degree of reaction of 87% produces approx. 23 g of portlandite [30]. "CH/23" therefore represents the proportion of cement in the concrete sample, assuming a hydration degree of 87% and no leaching.

$$\underline{C} = \frac{CH}{23} \cdot 100 \tag{6}$$

Finally, the % of aggregate (A) can be approximated using Equation (7):

$$A = 100 - \underline{C} \cdot (1 + w / c) \tag{7}$$

where w/c is the water-to-cement ratio of the concrete.

Cold water extraction (CWE) – pH calculation

Cold water extraction (CWE) can be used to determine the free alkali metal content per mass of concrete and the pH of the pore solution if the free water content is known [5]. However, aggregates can also release alkali metals during CWE, which can lead to an overestimation of the free alkali metal content of the concrete. To correct the results obtained for the concrete, the contribution of the aggregates must be known, so CWE was also performed on the aggregates extracted from the concrete (location E).

For CWE, 20 g of powder with a maximal grain size of 80 µm (both for the concrete and for the aggregate alone) was mixed with 20 g of deionized water (with a resistivity of 18.2 MΩ.cm) and stirred for 5 minutes. The suspension was then filtrated for approx. 1 minute using a water pump and a Grade 40, 8 µm particle retention Whatman cellulose filter. Preliminary investigations showed no significant uptake of ions by the filter [5]. Finally, each solution was diluted 10 times with deionized water and acidified with HNO_3 to obtain a final [HNO_3] concentration of 0.1 mol/l. The solutions were analysed for Na and K using Inductively Coupled Plasma Mass Spectrometry (ICP-MS). The method was applied twice for each sample, and a third measurement was performed if the two first measurements presented a too large difference (i.e. above 10 %).

As shown by Plusquellec et al. [5], using deionized water for the extraction of ions during CWE does not allow the determination of the calcium concentration in the pore solution of the samples due to the dissolution of portlandite ($Ca(OH)_2$) during the process. This can be avoided by replacing water with methanol during CWE. This enables the investigation on calcium, but the use of methanol leads to only a partial extraction of the free alkali metal ions and therefore cannot be used alone.

Based on the ICP-MS results, the free alkali metal content (not yet corrected for the release from the aggregates during CWE) can be calculated as shown in Equation (8):

$$X_{conc} = [X]_{ps+extr} \cdot \frac{m_{ps} + m_{extr}}{m_{sample}} \quad (8)$$

where X is either Na or K, X_{conc} is the alkali metal content of the concrete (mmol/kg), $[X]_{ps + extr}$ is the concentration of X in the filtrate obtained from CWE (mmol/l), m_{ps} is the amount of pore solution in the sample (g), m_{extr} is the amount of extraction solution (deionized water or methanol) added during CWE (g), and m_{sample} is the mass of the sample (g). Since m_{ps} is much lower than m_{extr}, it can be neglected [5].

For the calculation of the pH, the original concentration of the alkali metals in the pore solution ($[X]_{ps}$) has to be calculated. $[X]_{ps}$ can be calculated using Equation (9):

$$[X]_{ps} = [X]_{ps+extr-aggr} \cdot \frac{m_{ps} + m_{extr}}{m_{ps}} \quad (9)$$

where $[X]_{ps+extr-aggr}$ is the concentration of X in the filtrate obtained from CWE (mmol/l) and corrected for the release of X from the aggregates during CWE. $[X]_{ps+extr-aggr}$ can be determined using Equation (10):

$$[X]_{ps+extr-aggr} = [X]_{ps+extr} - \frac{[X]_{aggr} \cdot m_{sample} \cdot A/100}{m_{extr}} \quad (10)$$

where $[X]_{aggr}$ is the concentration of X in the filtrate after performing CWE on the aggregates alone.

Once $[X]_{ps}$ has been obtained, the pH can be calculated using the geochemical model PhreeqC provided by the US Geological Survey (USGS) [31]. The activity coefficients of the species in solution were calculated using the Pitzer approximation, which is accurate for concentrated solutions. To fit the experiments, the temperature was fixed at 20 °C for the calculation. The database presented in Plusquellec [32] was used. The (calculated) alkali metal concentrations in the pore solution were used as input. The pH determination was thus based on the Na and K content and the moisture content.

Acid dissolution

The acid soluble alkali metal content was determined by mixing 5 g of the powdered samples with 50 ml of HNO_3, 1.4 mol/l, heated at 80 °C. The cement paste was entirely dissolved. After filtration, the solutions were diluted 10 times with deionized water and analysed by ICP-MS for Na, K and Ca. Because a partial dissolution of the aggregates was expected, the aggregates previously extracted were also investigated separately by this method to measure the amount of Na and K that were released. Only a selection of slices were analysed using this technique (Table 3).

Crack pattern and crack density

Fluorescence-impregnated plane-polished sections of 90 x 300 mm were prepared from each location following the procedure described in Danish Standard DS 423.39 [33]. Pictures of the plane-polished sections were taken under UV light, revealing the crack pattern. The crack density was measured using ImageJ software on each plane-polished section as a function of its depth below the reference surface. After RGB separation, the cracks were selected by thresholding the green image. The crack density (i.e. the area of the cracks divided by the total area) was measured by ImageJ. Unfortunately, ImageJ counts any air voids as cracks after thresholding, and shadow effects enlarge the cracks, leading to an overestimation of the crack density. To limit this, we manually removed these artefacts. All the different steps are illustrated in Figure 4.

Elemental scanning

The four plane-polished sections were analysed by micro-XRF using an M4 Tornado from Bruker equipped with an Ag X-ray tube and two SDD detectors. For each sample, 15 areas of 10 mm width were mapped with a pixel size of 40 µm and an analysis time of 2 ms/pixel. After mapping, the software allows

differentiation of the two “phases”, the aggregates and the paste. The differentiation is based on the calcium content. K and Na were quantified in the paste of each area to obtain an alkali profile.

Alkali metal inventory

In addition to elemental profiles, the alkali metal contents obtained from CWE also made it possible to estimate an “alkali metal inventory” for the concrete, i.e. an estimation of its origination (cement, aggregate, ingress) and current location (pore solution, solid phase, leached).

The values obtained from CWE were first converted to kg/m^3 Na_2O_{eq} of concrete:

$$Na_2O^*_{eq,conc} = \frac{M(Na_2O)}{2} \cdot (Na_{conc} + K_{conc}) \cdot \rho_{conc} \quad (11)$$

where $Na_2O^*_{eq,conc}$ is the alkali metal content measured using CWE on the concrete sample in kg/m^3, $M(Na_2O)$ is the molar mass of Na_2O (0.06198 kg/mol), Na_{conc} and K_{conc} are the Na and K contents of the sample expressed in mol/kg (calculated with (3)), and ρ_{conc} is the concrete density in kg/m^3. To simplify the notation, all values obtained from CWE are annotated with *.

The values obtained using Equation (11) include the alkali metals released by the aggregates during CWE and therefore need to be corrected for that. To estimate the aggregate contribution, one needs to know the amount of aggregates in the sample. The original mix-design of the concrete used in the slab dam is known, but the aggregate content of the samples had to be checked using TGA (see above) because the composition of the concrete could vary from one location to another. To correct the $Na_2O^*_{eq,conc}$ for the alkali metal release from the aggregate during CWE, all the aggregates (fine and coarse) were assumed to

release the same amount of alkali metals (Table 5). However, the micro-XRF scanning revealed that the coarse aggregates are richer in K than the fine aggregates (see Figure 9), which could therefore result in an overestimation of the correction. The following formula was used for the correction:

$$Na_2O^*_{eq,conc-aggr} = Na_2O^*_{eq,conc} - \frac{m_{aggr}}{m_{conc}} \cdot Na_2O^*_{eq,aggr} \quad (12)$$

where $Na_2O^*_{eq,aggr}$ is the release of alkali metals measured using CWE on the aggregate sample and calculated using Equation (11), m_{aggr} is the mass of aggregates in 1 m^3 of concrete, and m_{conc} is the mass of 1 m^3 of concrete. $Na_2O^*_{eq,conc-aggr}$ represents the amount of free alkali metals in the concrete, i.e. present in the pore solution.

The correction could not, however, be applied to the samples from the surface of the cores due to the decrease in the portlandite content measured using TGA (see section 3.2). The decrease would lead to an unknown modification of the paste and aggregate content.

$Na_2O^*_{eq,conc-aggr}$ includes not only the alkali metals originating from the cement itself, but also any alkali metals which have been released over time to the pore solution by the aggregates. To differentiate these two categories, we can calculate what the alkali metal ion content in the pore solution would have been if no aggregates were present. Various studies have stated that, for a CEM I cement, approx. 50–70% of the total alkali content originating from the cement is present in the pore solution, while the rest is part of the solids, either sorbed on hydrates or still present in unreacted clinker phases [5, 8, 34]. The free alkali metal content in the pore solution $Na_2O_{eq,cem,ps}$, is therefore only a portion k_{free} of the total alkali metal content in the concrete $Na_2O_{eq,conc}$ originating from the cement.

$$Na_2O_{eq,cem,ps} = k_{free} \cdot Na_2O_{eq,conc} \quad (13)$$

$$Na_2O_{eq,conc} = \%Na_2O_{eq} \cdot \frac{m_{cem}}{V_{conc}} \quad (14)$$

where m_{cem}/V_{conc} is the mass of cement per cubic metre of concrete, and $\%Na_2O_{eq}$ the alkali content of the cement.

Finally, we can calculate the release:

$$Na_2O_{eq,release} = Na_2O^*_{eq,conc-aggr} - Na_2O_{eq,cem,ps} \quad (15)$$

In this approximation, it is assumed that all the alkali metals released by the aggregates were present in the pore solution and were not bound in the solid phase.

3. Results

The figures in this article refer to the “reference” surfaces of the core. These correspond to the “external” surfaces of the cores from locations W and WA (i.e. the ones in contact with the water reservoir), and to the north surface of the cores from location A and S (see Figure 1).

3.1. Moisture state

Figure 5 shows the measured degree of capillary saturation (DCS) given as a function of the distance from the reference surface of the cores. The data points cover the full length of the cores, but not the entire core. The length of each sample is indicated with a horizontal bar. Corresponding results for the internal relative humidity (RH) are shown in Figure 6. Table 4 presents the measured free water content or pore solution (W), present in the concrete. Each single data point represents results from one disc of concrete split from a concrete core. Thus, statistical analysis such as standard deviation of the data is not available. The accuracy of DCS and RH measurements is presented in the methods section.

All the DCS values presented in Figure 5 are in the range 82–98%. As expected, the highest water saturation was obtained in location W (lower part of the slab), with DCS > 91% throughout the entire core. Only the discs from the expected driest location S (pillar sheltered from rain) have DCS < 90% throughout the entire core (varying from 82% to 90%). The DCS in location A (exposed to rain) ranges between 87% and 95%, which is in the same range as the upper part of the slab (location WA) with DCS ranging from 85% to 92%. Moreover, the cores from locations A and S show a clear moisture profile with a wetter middle part and a significantly lower DCS towards both surfaces of the pillar. The core from location WA does not present a similar moisture profile. It was expected that the DCS would be highest towards the exposed surface of the submerged core (location W), but this was not the case. Probably, this is because the reservoir was emptied in preparation for the repair work several months before the sampling, resulting in the drying of the surface (this is also the case for the periodically submerged location WA). If we exclude the first measurement point of the core from location W, an increase in the DCS towards the upstream face (waterside) of the slab is observed.

Figure 6 shows that the RH for the different cores varies in the range from 83% to 95%. As for DCS, a clear RH profile can be observed for the core from location S (RH ranging from 83% to 90%, with lower values towards both surfaces) and for the core from location W (RH ranging from 83% to 95%, with highest values towards the external surface facing the upstream side of the slab). No clear RH profiles can be observed in location A and WA. It should be noted that the RH measured in the outermost samples facing the inside of the slab dam with the same environmental conditions (i.e. the last measurement points in location W and WA and the first and last measurement points in location S) show comparable values (83–85%). This finding indicates a pretty good accuracy of the RH measurements.

The relationship between the moisture state and the extent of ASR is discussed by Lindgård [35] and Larive et al. [36]. Their conclusion is that more access to moisture will normally lead to more ASR, provided that the alkali content of the concrete is similar (i.e. that no alkali leaching has taken place in part of the cross-section). In all the four locations at Votna I, RH is higher than the "accepted" lower critical limit for initiating ASR found in the literature, i.e. 80% [1]. Nevertheless, based on the RH and DCS values measured, we expected that the extent of ASR would be least in location S (pillar sheltered from rain).

As shown in Table 4, the overall water content in the four concrete cores varies in the range 4.5 – 6%wt (of dry concrete). No distinct profiles could be observed. Please note that these values depend on the paste-to-aggregate ratios in the different discs cut from the cores.

3.2. Thermogravimetric analysis

The results obtained using TGA on the powdered slices taken from cores W, WA, A, and S are presented in Figure 7 and Figure 8. The cores were analysed over their entire length.

Figure 7 shows the carbonate content of all the samples as a function of the distance from the reference surface. All the cores present the highest carbonate content at their extremities. The core from location S presents a higher carbonate content at both surfaces (5–6%) than those from the other locations (1.5 – 2.5%). This indicates that the higher DCS levels for W, WA, and A (Figure 5) limit the carbonation of the concrete surfaces. The conditions at location S allow slightly more carbonation, but only to a limited extent because the carbonation depth was less than 10 mm after approx. 50 years (estimation based on the carbonate content).

Figure 8 shows the portlandite content as a function of the distance from the exposed surface. In the middle of the cores, W and WA seem to have slightly higher portlandite content (approx. 4.5%) than A and S (approx. 3%). This indicates that the concrete used in the pillars contains less cement than the concrete used in the slab dam, as was also pointed out by the owner. Except for A, all the cores show significantly lower portlandite content in the surfaces of the cores. For all cores, relatively steady plateaus are reached, indicating that the aggregate-to-paste ratio is similar in the different slices. The lower portlandite content observed at both ends of the cores can be explained by carbonation, alkali leaching and/or a higher aggregate-to-paste ratio.

3.3. Micro-XRF

With a micro-XRF, it is possible to distinguish paste and aggregates as different phases using elements such as Ca. Figure 9 presents a photo of the sample retrieved from location S and the corresponding phase map (see section 2.2). The scanning was carried out on the first 150 mm of the cores.

To avoid the influence of alkali metals present in the aggregates, Na and K profiles were determined in the paste “phase” as a function of depth for all locations. Figure 10 presents the profiles. A decrease in K

towards the surface is observed for all locations, indicating leaching. The decrease is more pronounced for locations W and WA. The Na profiles show a similar trend, but less pronounced. This might be partly because Na is more difficult to analyse with this technique than K, due to its lower molar mass. The impact of the environmental conditions is illustrated, with more significant alkali metal leaching in immersed conditions. CWE was carried out to quantify the extent of alkali leaching.

3.4. Cold water extraction (CWE) – pH calculation

Aggregates

Table 5 summarizes the amount of alkali metals released from the coarse aggregates during CWE. The aggregates tested were extracted from the concrete sample taken from location E. The conversion to Na_2O_{eq} (kg/m^3, see eq. (9)) considered an aggregate density of 2700 kg/m^3. When taking into account the composition of the aggregates given in Table 1, 0.5%wt of the total of Na and K present in the aggregates were extracted during CWE.

Concrete

Figure 11 presents the alkali metal (Na, K) and Ca profiles obtained using CWE on samples from the four locations W, WA, A, and S. The data points cover the full length of the cores and are raw data, i.e. not corrected for the alkali contribution of the aggregates.

The alkali metal profiles obtained from W and WA are similar: a plateau is observed in the middle of the core (between approx. 10 cm and 40 cm from the reference surface, though with a larger deviation in the results observed for WA) and the alkali metal content decreases at both ends. This is similar to the profiles obtained by micro-XRF (Figure 9). The values of the plateau and the values at the surfaces are similar for W and WA, approx. 25 mmol/kg concrete for Na and approx. 30 mmol/kg for K at the plateau and 5

mmol/kg concrete for Na and approx. 8 mmol/kg for K at the surfaces. The alkali metal leaching affects the cores until about 10 cm depth from the reference surfaces.

The alkali metal profiles of A and S also present a plateau in the middle of the cores, but the content was slightly lower than for W and WA: about 18 mmol/kg concrete for Na and 22 mmol/kg for K. This was expected because the concrete in the pillars (A and S) is believed to contain less cement than that used for the slab (W and WA). There is a difference in the distribution of the alkali metals at the surface of the cores A and S. Core A shows a slight decrease in both Na and K towards the surface, indicating leaching. The leaching is, however, less pronounced than that observed in the cores W and WA, with 14 mmol/kg concrete for Na and 16 mmol/kg concrete for K in the outermost sections. The core taken from location S is different from the others. The Na and K content decreases towards the surface, but the outermost points present a significant increase in the alkali metal content.

The Ca profiles are also plotted in Figure 11. These profiles were also obtained using CWE, but using methanol for the extraction instead of deionized water. All the samples show that the Ca content increases where the alkali metal content decreases, and vice versa. Only the last point of the core WA (625 mm deep) does not follow this pattern, which is in line with the fact that the solubility of portlandite increases with decreasing concentrations of Na^+ and K^+ in solution [37], leading to an increase in the free calcium concentration at the leached surface.

The reader should keep in mind that all the data in Figure 11 are raw data: the alkali metals potentially released by the aggregates during the CWE are included. If we assume about 80%wt of aggregates in the concrete (Table 2) and the release indicated in Table 5, the contribution of alkali metals from the aggregates during CWE is about 15–20% of the total alkali metals measured in the plateaus. However,

even if the data in Figure 11 overestimate the free ion content in the samples, the patterns observed are valid.

Figure 12 shows the calculated pH profiles in the different locations (W, WA, A, and S). The calculation is based on the free alkali metal content corrected for the contribution of alkali metals from the aggregates during CWE.

The calculated pH for the outermost points of the cores are erroneous (represented with the empty markers in Figure 12). This is because we cannot properly correct the free alkali content for the contribution of free alkali from the aggregates during CWE. In order to do that we would need the determination of the aggregate content using TGA, which is not possible in these outermost sections due to leaching of the portlandite and carbonation (Figure 7 and Figure 8). Moreover, the presence of carbonate ions in the pore solution would result in a lower pH. The core S, which was carbonated at both surfaces, would probably present a decrease in pH at both ends instead of an increase, as observed in Figure 12, if the carbonate ions in the pore solution were taken into account. Nevertheless, Figure 12 presents the pH calculated on all samples, including the surfaces (represented with the empty markers).

A plateau is observed for all the cores from about 10 cm from the reference surface. The pH value of the plateau is approx. 14 in cores from W and WA (from the slab), and slightly lower, approx. 13.8, in cores A and S (from the pillar). In cores from W and WA, the pH decreases towards the ends of the cores.

3.5. Acid dissolution

The acid soluble alkali metal content values of the samples are given in Table 6. They are converted to kg/m^3 Na_2O_{eq} (see Equation (11)) and are given as both raw data and corrected for the aggregate contribution (see Equation (12)). The CWE results are included for comparison.

Our expectation was that the acid soluble alkali metal content of concrete would reflect the total alkali metal content in the cement paste, because this method dissolves all the paste. This assumes, however, that the amount of acid soluble alkali metal from the aggregates would be negligible. In fact, as Table 6 shows, the aggregates released large amounts of alkali metals during acid dissolution, i.e. 6.7 kg/m^3 of aggregate, Na_2O_{eq}. This renders this method useless for the determination of the total alkali metal content of the paste, as has also been observed in a recent study [38].

3.6. Crack pattern and density

Figure 13 shows the crack patterns in the four cores after image analysis, and Figure 14 gives the crack density of each plane-polished section as a function of its depth below the reference surface. We did not investigate the full length of the cores, but only the first 300 mm from the reference surface. Both figures show that, in all cores, fewer cracks are visible near the surface than further in. Furthermore, all the samples present cracks perpendicular to the reference surface. A plateau is also visible in all samples. The plateau is reached between 100 mm and 150 mm depth for W, WA and A, which corresponds to the position of the plateau determined using CWE. The plateau seems to be reached at less depth for core S, i.e. around 50 mm from the reference surface.

The alkali metal content seems to match the crack pattern: more cracks are observed where alkali metal content is highest (i.e. where there is no leaching). However, the local increase in the alkali metal content at the surface of core S is not reflected in Figure 13 and Figure 14.

4. Discussion

4.1. Impact of the environment on the free alkali content and damage

The lower critical limit of RH for initiating ASR found in the literature is about 80% [1]. An RH above 85% was measured over the entire length of the cores for all the different exposure conditions, except the reference surface of core S (82% RH) (Figure 6). This shows that a sufficient amount of water was present in the concrete to allow ASR. However, more access to moisture will normally lead to more ASR, provided identical alkali content, [35, 36]. The coarse aggregates used in the dam, from a local cataclasite rock, are potentially reactive. The variation in the alkali metal content is therefore a key parameter determining the extent of ASR.

For easy comparison of the alkali metal profiles obtained from CWE (Figure 11), the Na and K contents (mmol/kg) have been converted into kg/m^3 Na_2O_{eq} (see Equation (11)). Figure 15 gives a comparison of all the profiles not corrected for the contribution of the aggregates.

The external surfaces of cores W, WA, and A were affected by alkali metal leaching to a depth of approx. 10 cm, which is similar to what Kagimoto et al. [20] observed on a 14-year-old concrete structure. The alkali leaching was more pronounced towards the external surfaces of cores W and WA (upstream face of the slab) than in the case of the core A. The free alkali content decreased by approx. 75% between the bulk of the core (100–400 mm depth) and the surface (0–10 mm depth) in cores W and WA. There was

also a decrease in the free alkali metal content towards the internal surfaces of cores W and WA. This can partly be explained by leaching induced by the condensation of water on the walls inside the dam. However, an assumed higher aggregate-to-paste ratio towards the downstream face of the slab will also reduce the alkali metal content. At location A, leaching was observed from both (external) surfaces. The decrease in the free alkali metal content between the bulk of the core (100–350 mm depth) and the surface (0–50 mm depth) ranges between 25% and 50%. The reduced leaching observed for this location compared with locations W and WA might be explained by the fact that none of the surfaces at location A were submerged, just exposed to rainfall.

Because there are more alkali metals in the bulk than in the surface, ASR can be expected to be more pronounced in the bulk. This is in agreement with the observed crack density profile (Figure 14): there are more cracks in the bulk. Figure 16 shows the crack intensity in function of the alkali content. In general, the crack intensity seems to increase with the alkali content for the locations W, WA and A, but this is not the case for locations S.

For location S, an increase in the Na and K content is observed at the surface. Similar alkali metal accumulations have been attributed by Nixon et al. [39] and Åhs [40] to the evaporation of water from the material and the movement of water towards this drying zone. This mechanism is often referred to as “wick action”. The accumulation of free alkali metals near the surface is not reflected in a higher cracking density at the surface (see Figure 14). This is not surprising because “wick action” is also associated with drying and therefore lower RH (Figure 6). The reason why such alkali metal accumulation near the internal surface was not observed for W and WA is not known, but perhaps local moisture differences (even though similar RH values were measured in Figure 6) or large intervals in the alkali profiles may play a role.

The expansion of the concrete due to ASR in the bulk produces tension in the surface, leading to a map cracking pattern on the surface typical for ASR (cracks perpendicular to the surface). Generally for ASR-affected structures, less ASR-induced cracking (in particular cracks running from an aggregate particle, through the cement paste and continuing into the next aggregate particle) is observed in the outer part of a concrete core than in the bulk [22]. The difference in crack densities observed between the bulk and the surface could indicate an expanding core and an outer skin which expands less. To what extent this "skin action" can be attributed to alkali leaching is unclear, but the skin thickness seems to agree with the thickness of the leached zone. A greater expansion in the bulk than in the outer skin should lead to fewer but wider cracks in the skin than in the bulk [41]. In the samples taken from the dam, fewer cracks were observed in the skin but they were not wider than the cracks in the bulk. This might be due to the limited sample size (90 mm or 150 mm in the current study) only showing a couple of cracks in the outer skin of each section. Another influencing factor is that the width of surface cracks measured on drilled cores after arriving to the laboratory are often less than the crack width measured on the concrete surface before coring [22]. To be able to draw any conclusions on this, larger sections would need to be investigated to gain a more representative view of the number and size of the cracks.

4.2. Alkali metals inventory

In this section, we evaluate the amount of alkali metals that might have been released by the aggregates in the pore solution. The release is an important parameter because an increase in the free alkali content will enhance the alkali–silica reaction.

We use only the free alkali metal content (CWE) data obtained from the bulk. As an example for the estimation of the amount of alkali metals released from the aggregate, we chose core W and the slice located at a depth of 200 mm from the surface facing the water reservoir.

Using TGA on this slice, we found an aggregate content (coarse and fine) of 73%wt concrete, which corresponds to the concrete mix-design (78%wt (Table 2)). The 5%wt difference has only a minor impact on the calculated $Na_2O_{eq,\ conc\text{-}aggr}$ (free alkali metal content corrected for the aggregate contribution during CWE) and corresponds to a variation of 0.1 kg/m^3 Na_2O_{eq}.

Table 7 summarizes the assumptions, and the measured and calculated values if alkali metal content of the cement is 1.28% and the proportion of free alkali metals k_{free} = 50%. Figure 17 gives a graphic representation of the calculation described in section 2.2 for the actual concrete. The impact on the inventory of the alkali metal content of the cement (1.19% or 1.28%) and the proportion of free alkali metals (50%, 60% or 70%) is presented in Figure 18 and Figure 19.

Figure 18 shows that the variation of alkali metal content of the cement (1.28% vs 1.19%) does not affect the results. In both cases, the amount of alkali metal released by the aggregates is estimated to be about 1.1 kg/m^3. In contrast, Figure 19 shows that k_{free} has a strong impact on the calculated release: the alkali metal release from the aggregates ranges from 0.2 (k_{free} = 70%) to 1.1 kg/m^3 (k_{free} = 50%) with an alkali metal content of the cement fixed at 1.28%. An accurate determination of k_{free} is therefore needed for a proper estimation of the release. This could be done for example by analysing a concrete sample made with a similar mix-design and cement but with inert and non-releasing aggregates (e.g. pure limestone) [8].

The authors are involved in a round-robin test in the RILEM committee TC 258-AAA. The round-robin test aims to measure the potential alkali metal release of various aggregates by immersing them in high alkaline solutions (0.7 molar NaOH and KOH solutions saturated with $Ca(OH)_2$ and with a solution-to-aggregate

ratio of 4), which will mimic the pH of a concrete pore solution. This method is called RILEM AAR-8 [42]. A cataclasite rock, i.e. similar to the coarse aggregate present in the Votna I dam, has been tested. Equilibrium was achieved after 26 weeks of immersion at 38 °C, with a release of 1.4 kg/m^3 of concrete. The result obtained using the RILEM AAR-8 method, however, is not representative of what would happen in a concrete, and a calibration is needed. Such a calibration could be achieved using the method suggested in this paper provided that the proportion of free alkali metals is known.

5. Summary and conclusions

Cores were drilled from the ASR-affected Votna I dam located in the south-western part of Norway. The cores were taken at different locations of the dam to investigate the influence of the environmental conditions on the free alkali metal distribution. The environmental conditions studied were: submerged (location W), periodically submerged (location WA), atmospheric (location A) and sheltered (location S). The internal surfaces of cores W and WA and the two surfaces of core S were exposed to the internal moisture of the dam with a relatively high humidity. Samples extracted from the four locations were analysed as a function of their depth using: TGA, micro-XRF, image analysis, cold water extraction (CWE), and acid dissolution. The moisture state was also investigated: RH, DCS and water content.

1) The acid dissolution was unable to measure the alkali content due to the partial dissolution of the aggregates. However, CWE enabled us to determine the free alkali metal content of the different cores as a function of distance from the surface, highlighting the leaching of alkali metals. The leaching of K was also found using micro-XRF, which gave profiles similar to CWE.

2) The exposure conditions have an impact on the free alkali metal content:

- The external surfaces of the cores permanently submerged (location W) or periodically submerged (location WA) were affected by alkali metal leaching. The leaching profiles are similar. Leaching affects the concrete in the first 100 mm from the external surface.
- The external surfaces exposed to atmospheric conditions (e.g. rain or snow, location A) were also affected by leaching, but to a lesser extent than the submerged surfaces.
- For one of the internal surfaces, an accumulation of alkali was observed which might indicate wick action. The other internal surfaces also indicate alkali leaching.

3) The alkali metal profiles correspond relatively well to the crack density profiles: less ASR-induced cracking was observed in alkali-leached zones than in the bulk of the cores. However, it remains unclear to what extent this typical crack pattern can be attributed to alkali leaching.

4) The results obtained from CWE on the non-leached area of the core from location W enabled us to estimate the release of alkali metals from the aggregates to the concrete. With the information available on the Votna I dam, we estimated an alkali metal release ranging from 0.2 to 1.1 kg/m^3 Na_2O_{eq}, depending on the assumed proportion of free alkali metals in the pore solution (in the range 50-70 %).

6. Acknowledgments

The authors acknowledge the financial support from the project 236661/O30 “Alkali–silica reaction in concrete – reliable concept for performance testing”, managed by SINTEF Building and Infrastructure and supported by the Norwegian Research Council and industrial partners: Norcem, NorStone, Norsk Stein,

Hydro Energy, Axion, and the Norwegian Roads Administration. We are also very grateful to Havvagul Vurucu (NTNU), Tone Anita Østnor (SINTEF), and Anne-Kristin Mjøen (SINTEF) for their help during the experimental study. The authors also want to thank Marit Haugen (SINTEF) for her help with the plane-polished section analysis and for the documentation of the Votna I dam, Syverin Lierhagen (NTNU) for the ICP-MS analysis, and Torill Sørlokk (NTNU) for the XRF analysis. We are also very grateful to Benoit Fournier, Josée Duchesne and Mathieu Champagne (Université Laval), Børge Johannes Wigum (NTNU/Heildelberg Cement), and Max Hendriks for our fruitful discussions. The authors also acknowledge Lawrence White (Language Support Centre) for the proofreading.

7. References

[1] S.W. Tang, Y. Yao, C. Andrade, Z.J. Li, Recent durability studies on concrete structure, Cement and Concrete Research, 78, Part A (2015) 143-154.
[2] D. Stark, The moisture condition of field concrete exhibiting alkali-silica reactivity, Special Publication, 126 (1991) 973-988.
[3] A. Vollpracht, B. Lothenbach, R. Snellings, J. Haufe, The pore solution of blended cements: a review, Materials and Structures, 49 (2015) 3341-3367.
[4] M.C. Alonso, J.L. García Calvo, C. Walker, M. Naito, S. Pettersson, I. Puigdomenech, M.A. Cuñado, M. Vuorio, H. Weber, H. Ueda, K. Fujisaki, Development of an accurate pH measurement methodology for the pore fluids of low pH cementitious materials, 2012 111.
[5] G. Plusquellec, M.R. Geiker, J. Lindgård, J. Duchesne, B. Fournier, K. De Weerdt, Determination of the pH and the free alkali content in the pore solution of concrete: review and experimental comparison, Cement and Concrete Research, 96 (2017) 13.
[6] M.A.T.M. Broekmans, Structural properties of quartz and their potential role for ASR, Materials Characterization, 53 (2004) 129-140.
[7] Norwegian Concrete Association, Durable concrete containing alkali reactive aggregates, NB Publication No. 21, Oslo, (2004), 22 +12 including appendices (in Norwegian).
[8] C. Drolet, J. Duchesne, B. Fournier, Validation of the alkali contribution by aggregates to the concrete pore solution, Cement and Concrete Research, 98 (2017) 10-23.
[9] D. Constantiner, S. Diamond, Alkali release from feldspars into pore solutions, Cement and Concrete Research, 33 (2003) 549-554.
[10] K. De Weerdt, D. Orsáková, A.C.A. Müller, C.K. Larsen, B. Pedersen, M.R. Geiker, Towards the understanding of chloride profiles in marine exposed concrete, impact of leaching and moisture content, Construction and Building Materials, 120 (2016) 418-431.
[11] U.H. Jakobsen, K. De Weerdt, M.R. Geiker, Elemental zonation in marine concrete, Cement and Concrete Research, 85 (2016) 12-27.
[12] J. Lindgård, M.D.A. Thomas, E.J. Sellevold, B. Pedersen, Ö. Andiç-Çakır, H. Justnes, T.F. Rønning, Alkali–silica reaction (ASR)—performance testing: Influence of specimen pre-treatment, exposure conditions and prism size on alkali leaching and prism expansion, Cement and Concrete Research, 53 (2013) 68-90.

[13] J. Bokern, Concrete tests for ASR assessment: Effects of testing environment on preconditions for an ASR and transferability of test results, Proceedings of the 13th International Conference on Alkali-Aggregate Reactions in Concrete, Trondheim, Norway, 2008, 511-520.
[14] C.A. Rogers, R.D. Hooton, Reduction in mortar and concrete expansion with reactive aggregates due to alkali leaching, Cement, concrete and aggregates, 13 (1991) 42-49.
[15] M. Thomas, B. Fournier, K. Folliard, J. Ideker, M. Shehata, Test methods for evaluating preventive measures for controlling expansion due to alkali–silica reaction in concrete, Cement and Concrete Research, 36 (2006) 1842-1856.
[16] P. Rivard, M.A. Bérubé, J.P. Ollivier, G. Ballivy, Decrease of pore solution alkalinity in concrete tested for alkali-silica reaction, Materials and Structures, 40 (2007) 909-921.
[17] H. Vivian, Studies of cement-aggregate reactions—the effect of void space on mortar expansion, CSIRO Bulletin, 229 (1947) 55-56.
[18] P.E. Grattan-Bellew, A. Danay, Comparison of laboratory and field evaluation of alkali-silica reaction in large dams, International Conference on Concrete Alkali-aggregate Reactions in Hydroelectric Plants and DamsFrederiction, New Brunswick, Canada, 1992, pp. 1-25.
[19] M.-A. Bérubé, J. Duchesne, J.F. Dorion, M. Rivest, Laboratory assessment of alkali contribution by aggregates to concrete and application to concrete structures affected by alkali–silica reactivity, Cement and Concrete Research, 32 (2002) 1215-1227.
[20] H. Kagimoto, M. Sato, M. Kawamura, Evaluation of the degree of deterioration in ASR damaged concretes and analyses of their pore solutions, Journal of the Japan Society of Civil Engineers, 641 (2000) 241-252.
[21] S. Larsen, J. Lindgård, E. Thorenfeldt, E. Rodum, M. Haugen, Experiences from extensive condition survey and FEM-analyses of two norwegian concrete dams with ASR, Proceedings of the 13th International Conference on Alkali-Aggregate Reaction in Concrete, Citeseer, Trondheim, Norway, 2008.
[22] M.K. Haugen, Personal Communication, 2017.
[23] V. Jensen, Alkali aggregate reaction in Southern Norway, Division of Geology and Mineral Resources Engineering, Norwegian Institute of Technology, University of Trondheim, Trondheim, 1993.
[24] E. Rodum, J. Lindgård, E. Thorenfeldt, Dam I Votna – prøving av utboret betong, SINTEF report STF50 F05092, in Norwegian, 2005.
[25] M. Haugen, O. Skjølsvold, J. Lindgård, B.J. Wigum, Cost effective method for determination of aggregate composition in concrete structures, 12th ICAAR Conference, Beijing, 2004.
[26] E.J. Sellevold, T. Farstad, The PF-method – A simple way to estimate the w/c-ratio and air content of hardened concrete, Proceedings of ConMat'05 and Mindess Symposium. Vancouver, Canada: The University of British Colombia. ISBN 0-88865-810-0, 2005.
[27] J. Lindgård, E.J. Sellevold, M.D.A. Thomas, B. Pedersen, H. Justnes, T.F. Rønning, Alkali–silica reaction (ASR)—performance testing: Influence of specimen pre-treatment, exposure conditions and prism size on concrete porosity, moisture state and transport properties, Cement and Concrete Research, 53 (2013) 145-167.
[28] Vaisala Instruments Catalog, Ref B210768EN rev. A 2009, www.vaisala.com/HM44.
[29] K. Scrivener, R. Snellings, B. Lothenbach, A Practical Guide to Microstructural Analysis of Cementitious Materials, A Practical Guide to Microstructural Analysis of Cementitious Materials, Chapter "Thermogravimetric analysis" by Lothenbach, Drudzinski and De Weerdt, Crc Press2016.
[30] K. De Weerdt, M. Ben Haha, G. Le Saout, K.O. Kjellsen, H. Justnes, B. Lothenbach, Hydration mechanisms of ternary Portland cements containing limestone powder and fly ash, Cement and Concrete Research, 41 (2011) 279-291.
[31] S.R. Charlton, D.L. Parkhurst, Modules based on the geochemical model PHREEQC for use in scripting and programming languages, Computers & Geosciences, 37 (2011) 1653-1663.

[32] G. Plusquellec, Analyse in situ de suspensions de silicate de calcium hydraté: application aux interactions ioniques à la surface des particules, Université de Bourgogne, 2014.
[33] Fonden Dansk Standard, DS 423.39:2002 - Betonprøvning - Hærdnet beton - Fremstilling af fluorescensimprægnerede planslib, Göteborg, (2002), 8 (in
[34] H.F. Taylor, A method for predicting alkazi ion concentrations in cement pore solutions, Advances in Cement Research, 1 (1987) 5-17.
[35] J. Lindgård, Alkali-silica reaction (ASR)–Performance testing, PhD, NTNU, Trondheim, 2013.
[36] C. Larive, A. Laplaud, O. Coussy, The role of water in alkali-silica reaction, Alkali-aggregate reaction in concrete, Québec, Canada, (2000) 61-69.
[37] J. Duchesne, E.J. Reardon, Measurement and prediction of portlandite solubility in alkali solutions, Cement and Concrete Research, 25 (1995) 1043-1053.
[38] P.H. Kermit, Determining alkali content in ASR performance-tested concrete, MSc, NTNU, Trondheim, 2017.
[39] P.J. Nixon, R.J. Collins, P.L. Rayment, The concentration of alkalies by moisture migration in concrete - a factor influencing alkali aggregate reaction, Cement and Concrete Research, 9 (1979) 417-423.
[40] M. Åhs, Redistribution of moisture and ions in cement based materials, Lund University, 2011.
[41] M. Hendriks, Personal Communication, 2017.
[42] RILEM, Determination of Alkalis Releasable by Aggregates in Concrete (draft Frebruary 2014), 2016.

Tables

Table 1: Composition of the coarse aggregate (determined using XRF) and the water of the reservoir (determined using ICP-MS).

Coarse aggregate		Water from the reservoir	
Component	%wt	Component	µmol/l
Fe_2O_3	2.61	Ca	82
TiO_2	0.26	Mg	11
CaO	0.87	Na	34
K_2O	5.00	K	7
P_2O_5	0.03	S	11
SiO_2	72.94	Si	27
Al_2O_3	12.78	Mn	1
MgO	0.28	Fe	1
Na_2O	2.86		
MnO	0.02		
LOI 1000 °C	0.94		
Total	98.59		

Table 2: Mix-design of the concrete used in the main part of the slab dam, i.e. excluding the pillars (kg/m³).

	Cement	Sand (0–8 mm)	Coarse aggr. (8–50 mm)	Water
kg/m³	352	930	955	188

Table 3: Overview of samples and tests

Exposure	Name	Type	Methods used	Sampling*
Submerged in water	W	Core	CWE TGA Acid dissolution (slices 1, 6, 7, 8 and 10)	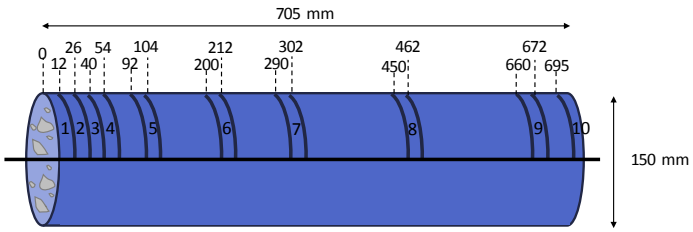
			Moisture	Discs 50 mm long, diameter 90 mm, taken at various depths (parallel cores)
			micro-XRF, crack pattern	Impregnated plane polished section, 90 x 300 mm, taken from the surface (parallel core)
	E	Block	Extraction of aggregates	pieces 100 x 100 x 100 mm
Periodically submerged	WA	Core	CWE TGA Acid dissolution (slices 1, 6, 7, 8 and 10)	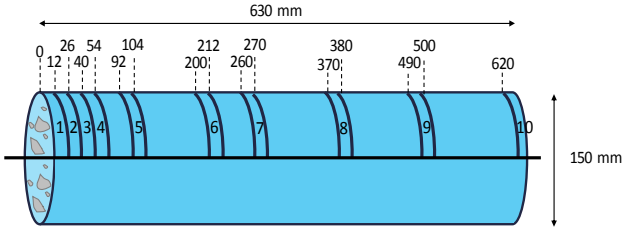
			Moisture	Discs 50 mm long, diameter 90 mm, taken at various depths (parallel cores)
			micro-XRF, crack pattern	Impregnated plane polished section, 150 x 300 mm, taken from the surface (parallel core)
Atmospheric conditions	A	Core	CWE TGA Acid dissolution (slices 1, 5, 6, 7 and 9)	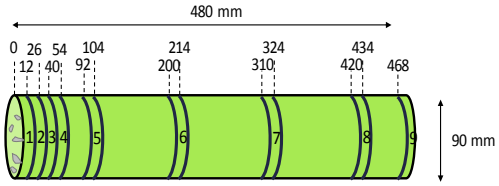
			Moisture	Discs 50 mm long, diameter 90 mm, taken at various depths (parallel cores)
			micro-XRF, crack pattern	Impregnated plane polished section, 90 x 300 mm, taken from the surface (parallel core)
Sheltered	S	Core	CWE TGA Acid dissolution (slices 1, 5, 6, 7 and 9)	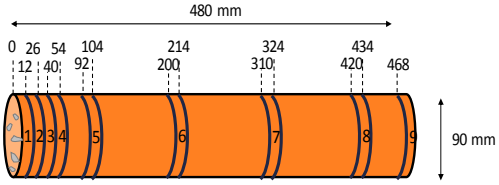
			Moisture	Discs 50 mm long, diameter 90 mm, taken at various depths (parallel cores)
			micro-XRF, crack pattern	Impregnated plane polished section, 90 x 300 mm, taken from the surface (parallel core)

* The black lines on the sketches represent where the cores were sawn

Table 4: Water content (W) as a function of the distance from the surface of the cores taken from locations W, WA, A, and S.

W		WA		A		S	
Distance (mm)	W (%wt)	Distance (mm)	W (%wt)	Distance (mm)	W (%wt)	Distance (mm)	W (%wt)
0–50	6.0	0–50	4.6	0–50	5.8	0–50	4.4
50–100	6.1	50–100	5.7	50–100	6.3	50–100	5.3
230–280	5.4	160–215	4.4	210–260	5.5	150–200	5.4
330–380	5.5	255–315	4.9	380–430	5.2	200–280	5.4
430–480	5.3	375–425	4.6	430–480	4.4	280–330	5.9
570–620	5.7	425–485	4.6			380–420	6.1
660–710	4.4	575–625	3.2			420–480	4.5

Table 5: Release of alkali metals from the coarse aggregates during CWE (average of three measurements and associated standard deviation)

Element	Release		Unit
	Average	Std. dev.	
K	5.2	0.3	mmol/kg
Na	4.7	0.2	mmol/kg
Na_2O_{eq}	0.8	0.04	Kg/m^3

Table 6: Sodium equivalent content Na_2O_{eq} obtained from applying CWE and acid dissolution to concrete and coarse aggregate samples. For the concrete, the middle two columns show values not corrected for the contribution from aggregates, while the last two columns (*) show the corrected values.

Location or sample	Depth	CWE	Acid	CWE*	Acid*
	Mm	Na_2O_{eq} – kg/m^3		Na_2O_{eq} – kg/m^3	
W	0–10	0.9	5.2	0.3	-1.5
	200–210	3.9	8.1	3.3	1.4
	290–300	4.0	8.7	3.4	2.0
	450–460	4.0	8.2	3.4	1.6
	695–705	1.3	7.5	0.6	0.8
WA	0–10	1.0	5.4	0.4	-1.2
	200–210	4.0	8.3	3.4	1.6
	260–270	4.0	8.7	3.4	2.0
	370–380	3.1	7.9	2.5	1.3
	620–630	1.1	7.2	0.5	0.5
A	0–10	1.7	7.9	1.7	1.3
	90–100	2.4	7.9	2.4	1.2
	200–210	2.6	7.7	2.6	1.1
	310–320	2.9	7.7	2.9	1.1
	470–480	1.5	9.1	1.5	2.5
S	0–10	3.0	11.9	2.3	5.3
	14–24	1.6	5.5	0.9	-1.2
	90–100	2.9	6.2	2.2	-0.5
	200–210	3.1	5.6	2.5	-1.1
	310–320	2.8	5.7	2.1	-1.0
	470–480	3.9	17.9	3.2	11.2
Aggregate	-	0.6	6.7	-	-

*corrected from the contribution from aggregates

Table 7: Alkali metals inventory – assumptions and results. Data obtained at location W, 200 mm below reference surface.

	Parameter	Definition	Value
Concrete mix-design	m_{cem}/V_{conc}	Cement content of the concrete	352 kg/m^3
	m_{aggr}/m_{conc}	Aggregate content of the concrete	78%
Assumptions	$\%Na_2O_{eq}$	Alkali metal content of the cement	1.28% and 1.19%
	k_{free}	Proportion of free alkali metals (i.e. in the pore solution)	50%, 60% and 70%
	ρ_{conc}	Concrete density	2425 kg/m^3
	ρ_{aggr}	Aggregate density	1885 kg/m^3
Measured	Na_{conc}	Na content of the concrete, uncorrected	23 mmol/kg
	K_{conc}	K content of the concrete, uncorrected	28.9 mmol/kg
	Na_{aggr}	Na released by the aggregates during CWE	4.7 mmol/kg
	K_{aggr}	K released by the aggregates during CWE	5.2 mmol/kg
Calculated ǂ	$Na_2O^*_{eq,\ conc}$	Free alkali metals content of the concrete	3.9 kg/m^3 Na_2O_{eq}
	$Na_2O^*_{eq,\ aggr}$	Alkali metals release from the aggregates during CWE	0.6 kg/m^3 Na_2O_{eq}
	$Na_2O_{eq,\ conc\text{-}aggr}$	Free alkali metals content of the concrete	3.3 kg/m^3 Na_2O_{eq}
	$Na_2O_{eq,\ cem,\ ps}$	Free alkali metals originating from the cement	2.3 kg/m^3 Na_2O_{eq}
	$Na_2O_{eq,\ release}$	Free alkali metals originating from the aggregates	1.1 kg/m^3 Na_2O_{eq}
	$Na_2O_{eq,\ solid}$	Alkali metals bound in the solid	2.3 kg/m^3 Na_2O_{eq}

ǂ: considering $\%Na_2O_{eq}$ = 1.28% and k_{free} = 50%

Figures

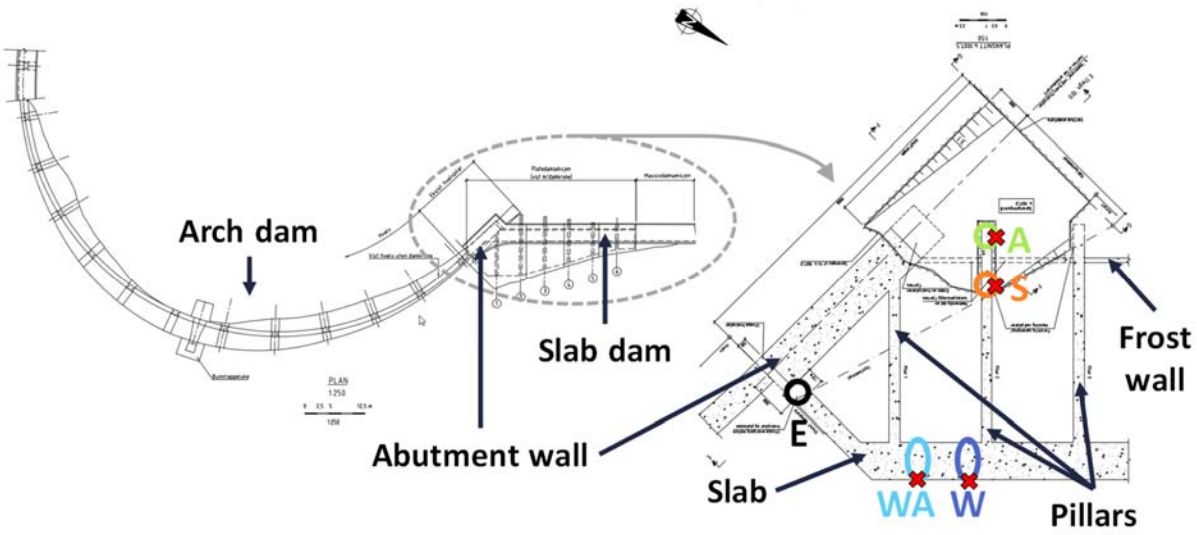

Figure 1. Sketch of the Votna I dam (top view) and location of the different cores (see Table 3). The crosses indicate the reference surface of the cores. The arrow at the top points north. Provided by Hydro Energy AS.

Figure 2. Photo of the Votna I dam (photo: J. Lindgård).

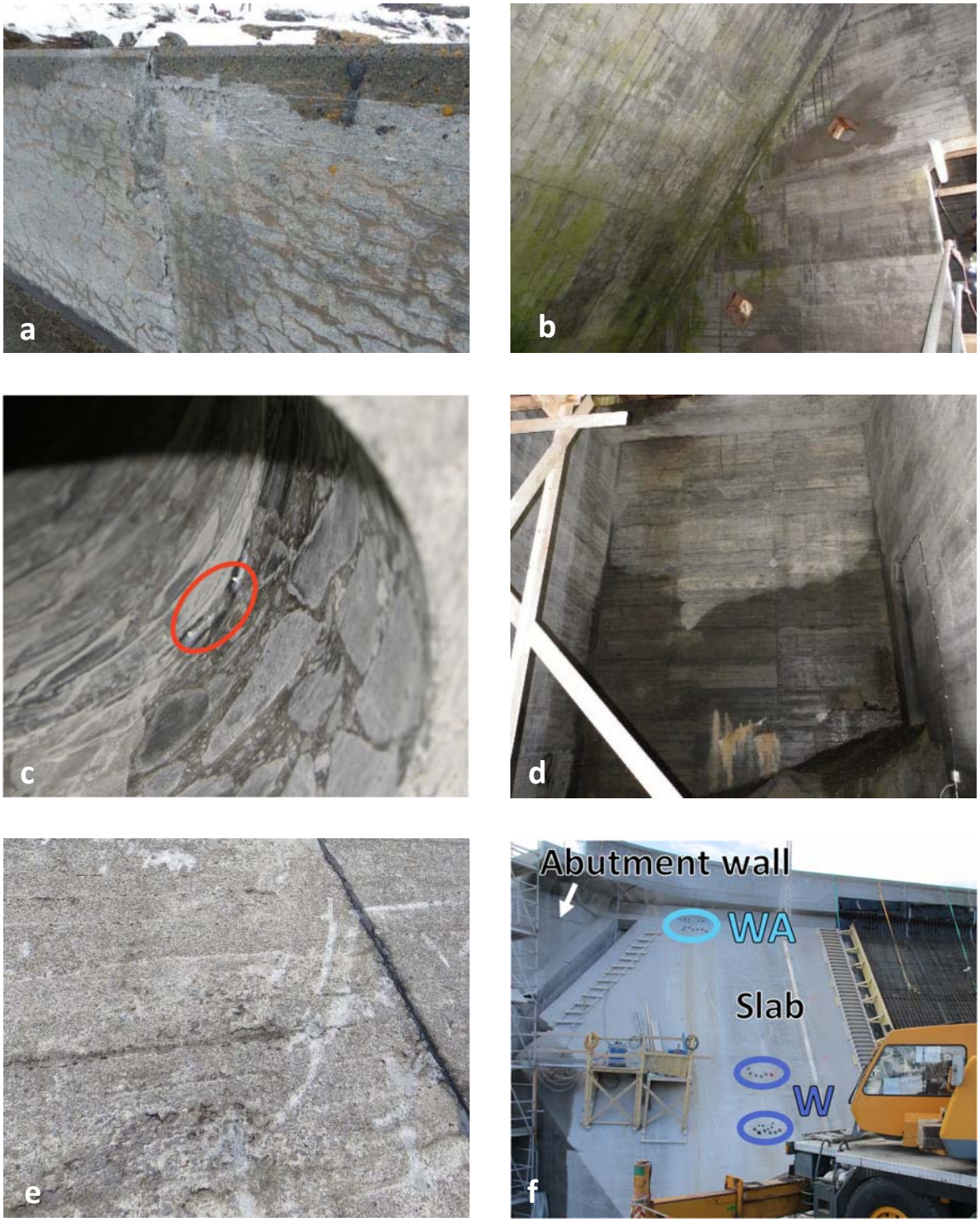

Figure 3. Photos of the Votna I dam at various locations: a) map cracking observed at the rail of the dam; b) map cracking observed inside the slab dam; c) presence of ASR gel in a bore hole in the dam; d) humidity inside the slab dam; e) aggregates visible on the surface of the concrete exposed to the reservoir (upstream face of the slab dam); f) upstream face after drilling of the cores and cutting of the blocks. May–June 2015 (photos a–e: G. Plusquellec; f: S.Å. Ekkje).

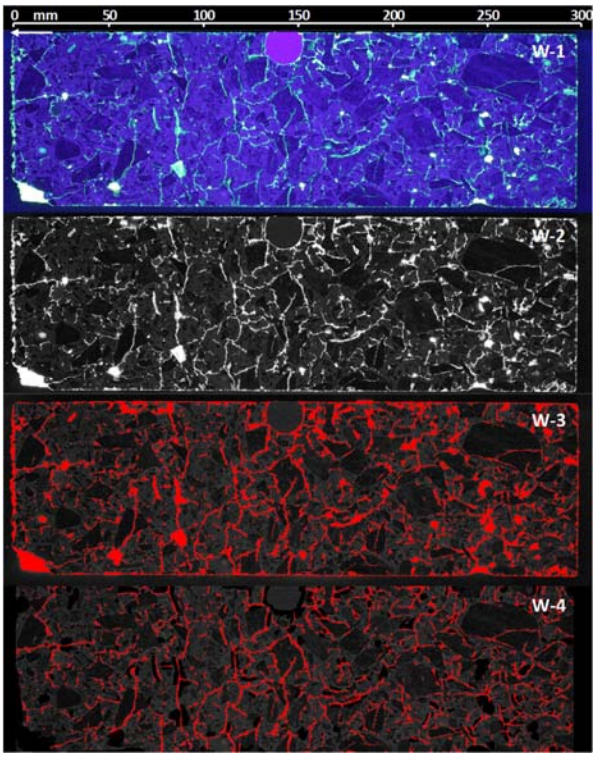

Figure 4: Determination of the crack pattern by image analysis. The four steps of the procedure are illustrated for location W: 1) photo of the sample in UV light; 2) "green image" of the previous photo after RGB separation; 3) thresholding of the green image, 4) removing of air voids and correction of the width of the cracks. The external surface is on the left-hand side of the picture.

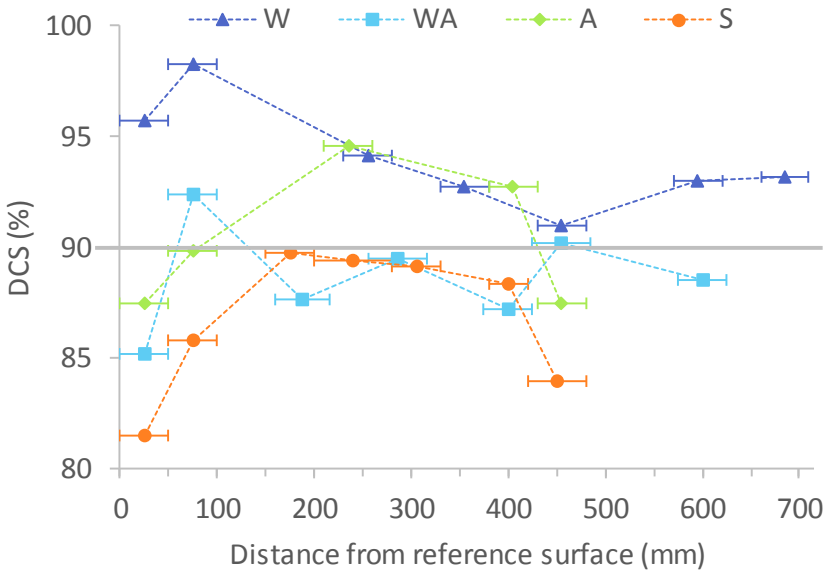

Figure 5. Degree of capillary saturation (DCS) versus the distance from the reference surface for locations W, WA, A, and S. The horizontal bars represent the thickness of the discs taken from each core.

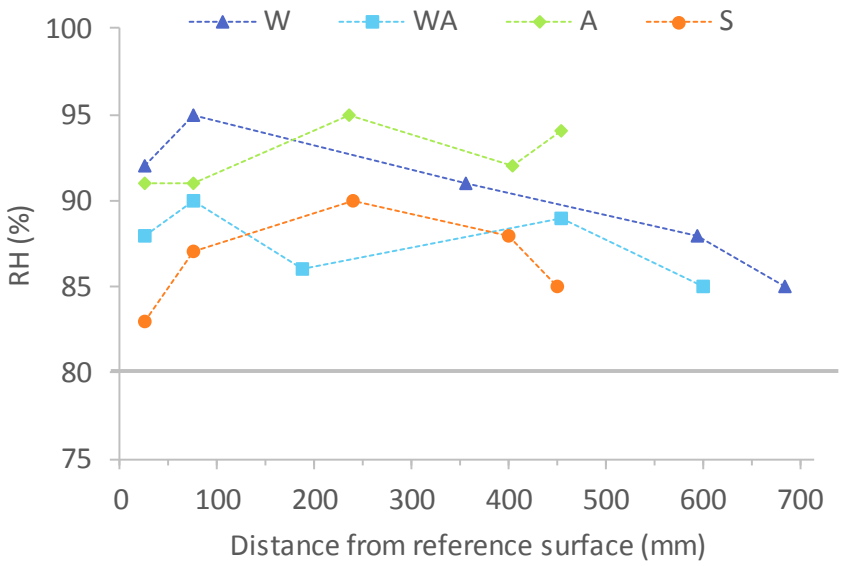

Figure 6. Relative humidity (RH) versus the distance from the reference surface for locations W, WA, A, and S.

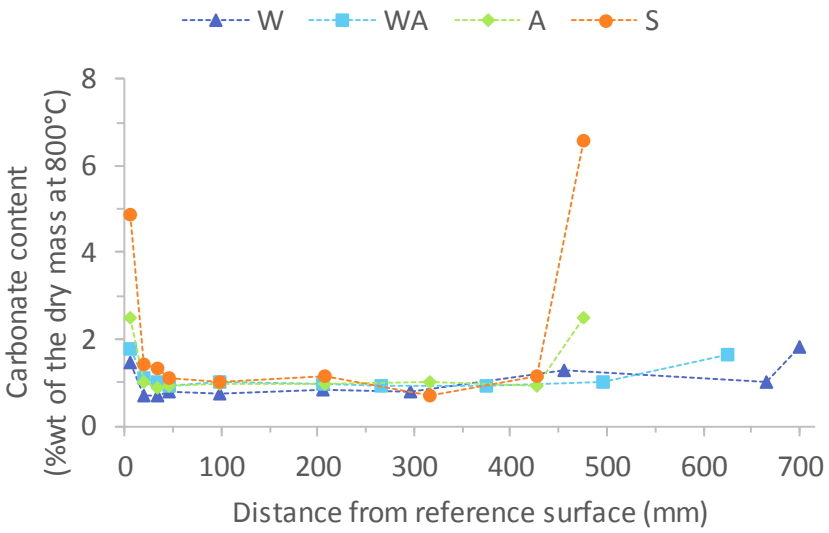

Figure 7: Carbonate content as a function of the distance from the reference surface of cores W, WA, A, and S.

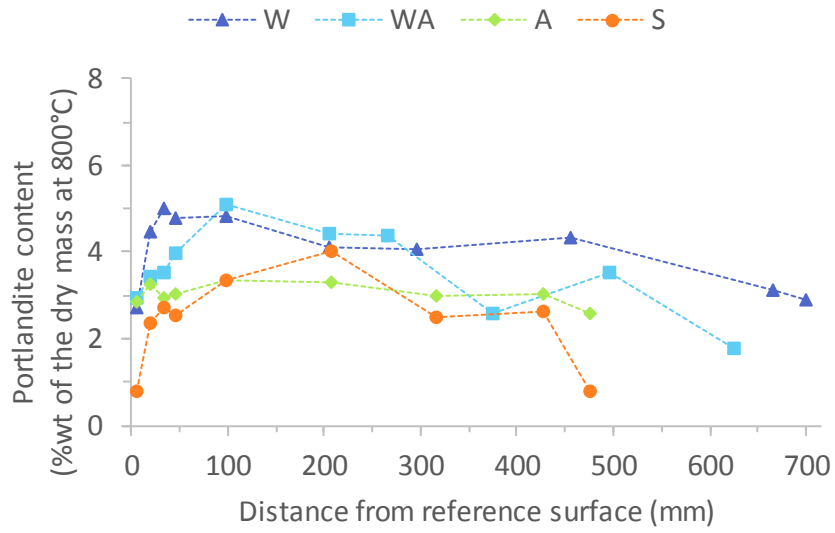

Figure 8: Portlandite content as a function of the distance from the reference surface of cores W, WA, A, and S.

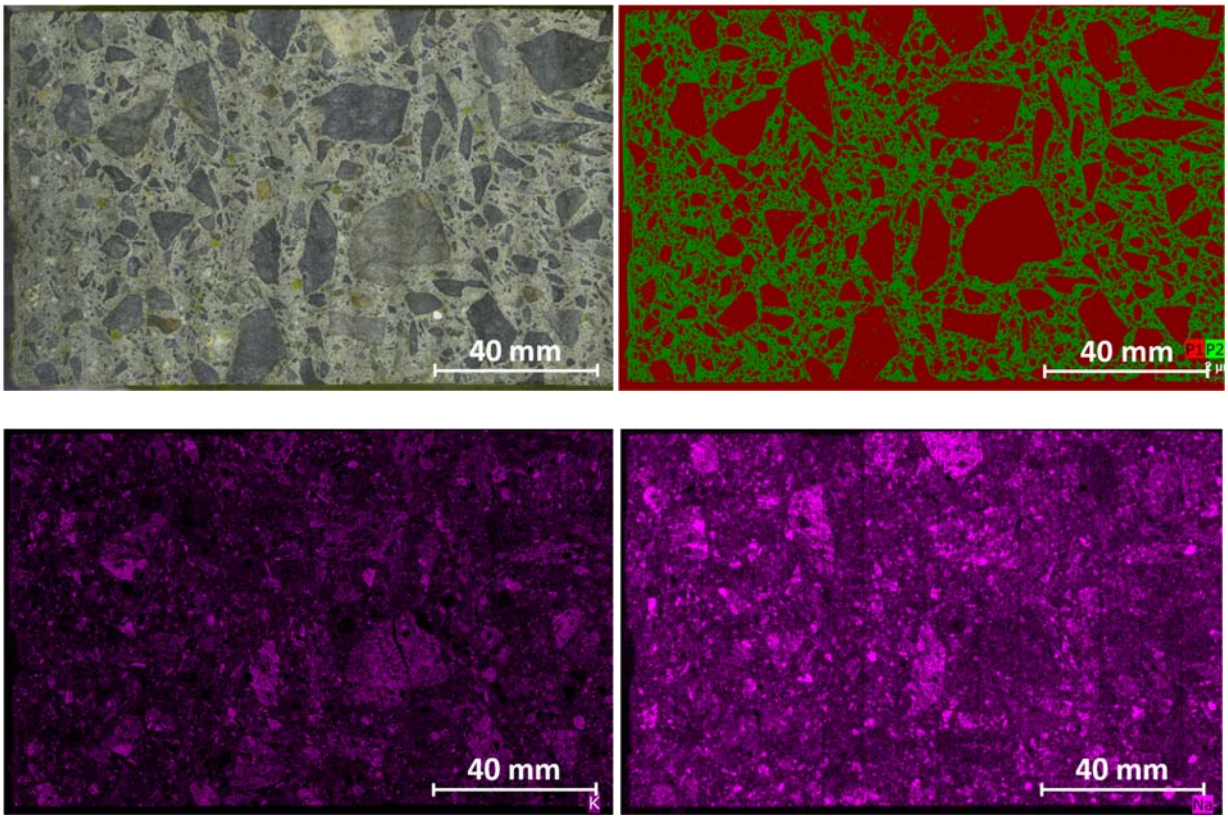

Figure 9: Example of a micro-XRF scanning on the plane-polished section prepared from location S. The top-left picture is a photograph of the sample. This area was divided into 15 areas (width of 10 mm) which were scanned. The top-right picture presents a montage of the phase analysis: the paste is in green, and the aggregates and voids are in red. The pictures at the bottom present the K (left) and Na (right) mappings of the sample.

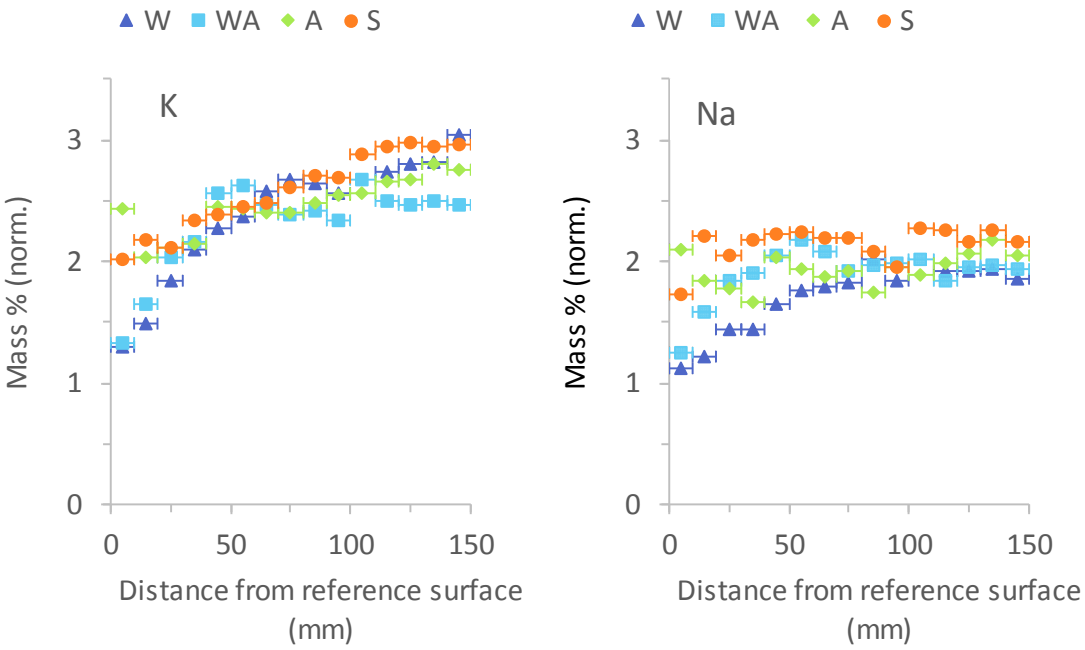

Figure 10: K (left) and Na (right) profiles measured in the paste (green phase in Figure 9) with the micro-XRF for the different locations. The measurements are normalized to the total mass of all the selected elements for the analysis (Ca, Na, K, Mg, Al, Si, P, S, Cl, Ti, Mn, and Fe).

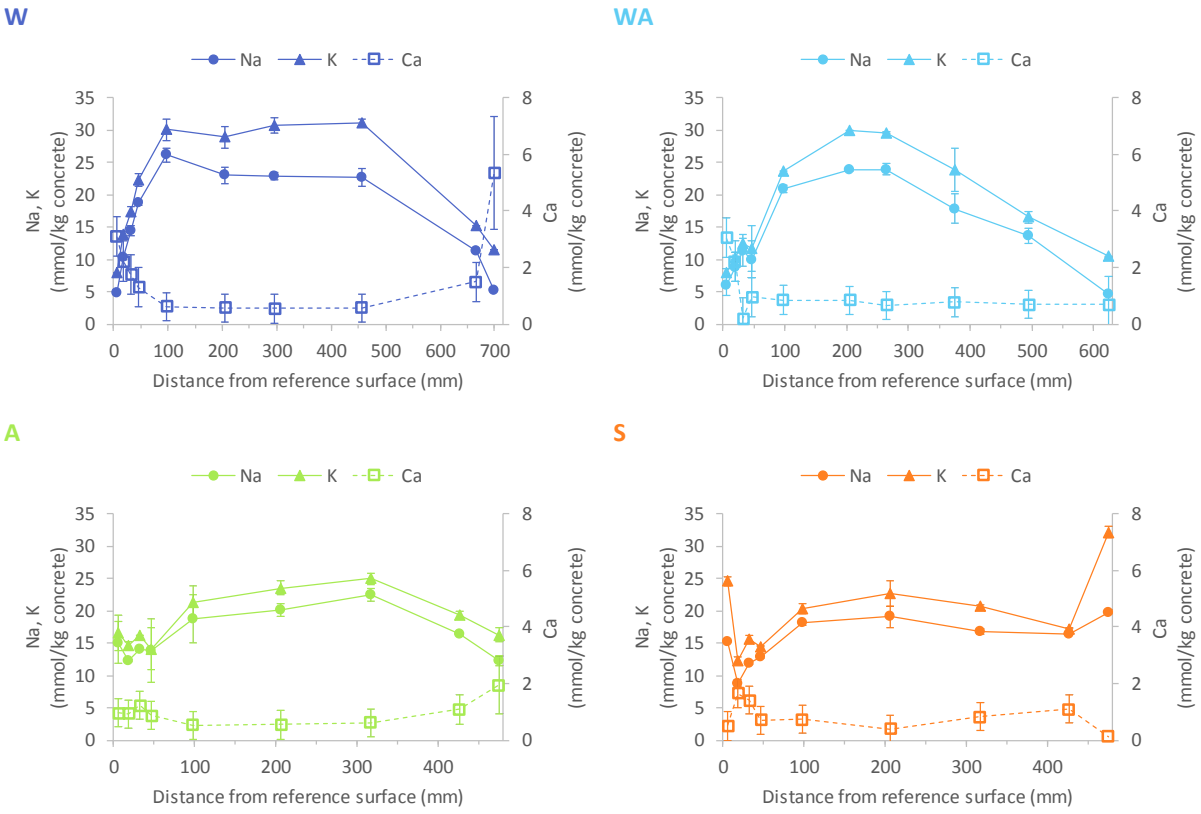

Figure 11. Na, K and Ca profiles (mmol/kg of concrete) as a function of distance from the reference surface obtained after CWE on cores W, WA, A, and S. The data are raw data, not corrected for potential alkali metal release from the aggregates. Each point is the average of two or three measurements, associated with the standard deviation (error bar).

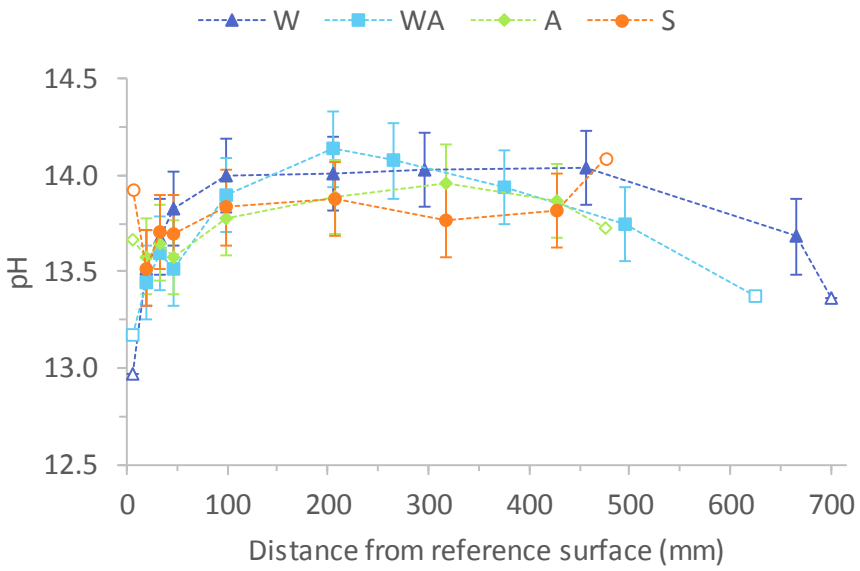

Figure 12. pH profiles as a function of distance from the reference surface of the cores taken from locations W, WA, A, and S. The points corresponding to the ends of the cores are hollow and not associated with an error bar because they do not reflect reality and are expected to be overestimated.

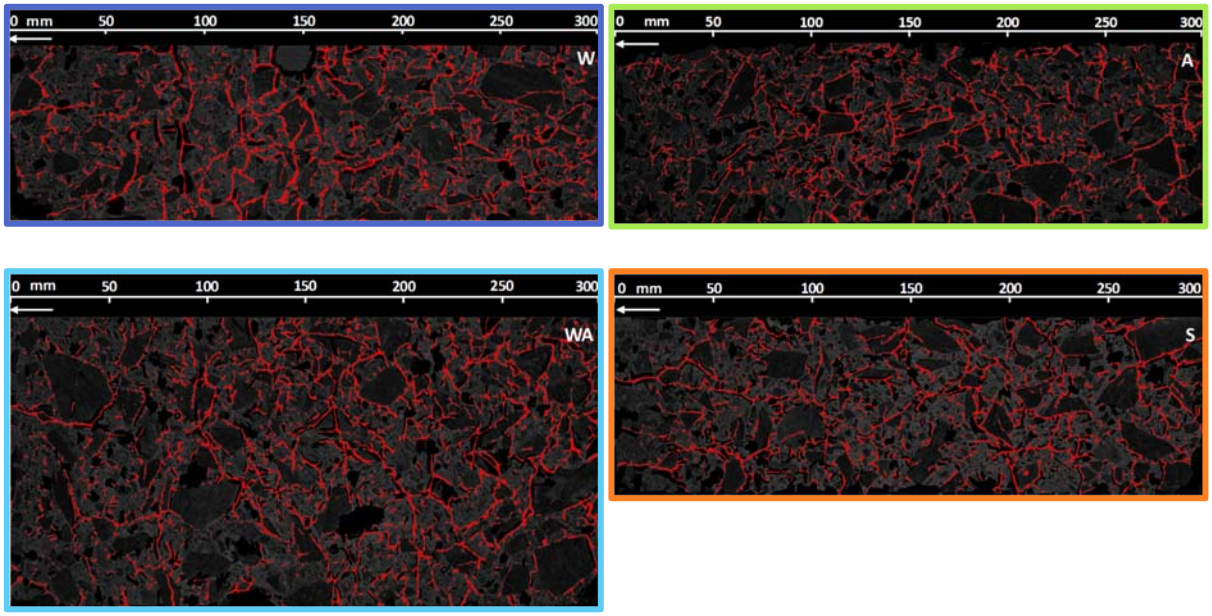

Figure 13: Crack patterns (obtained with ImageJ) from cores W, WA, A, and S.

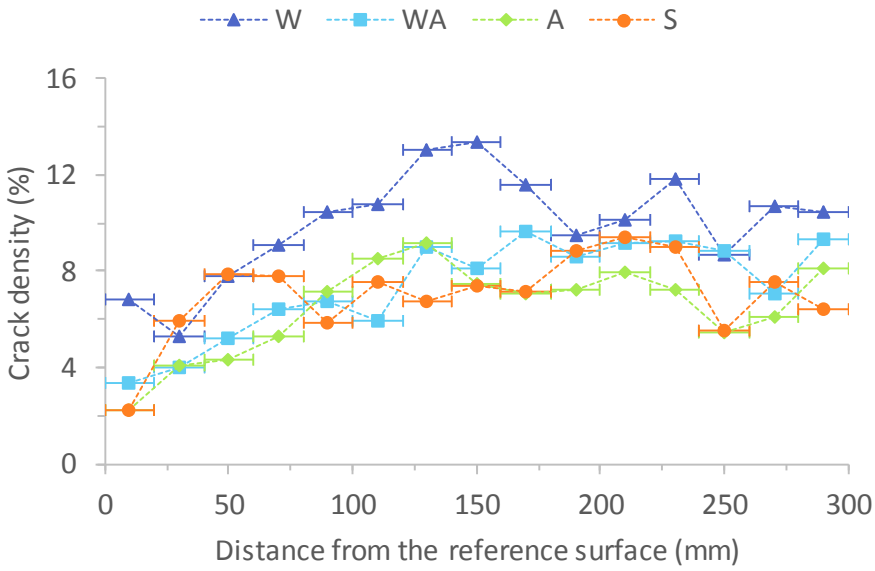

Figure 14: Crack density determined using ImageJ in function of the distance from the reference surface in the four cores. The horizontal bars represent the length of the core taken into account.

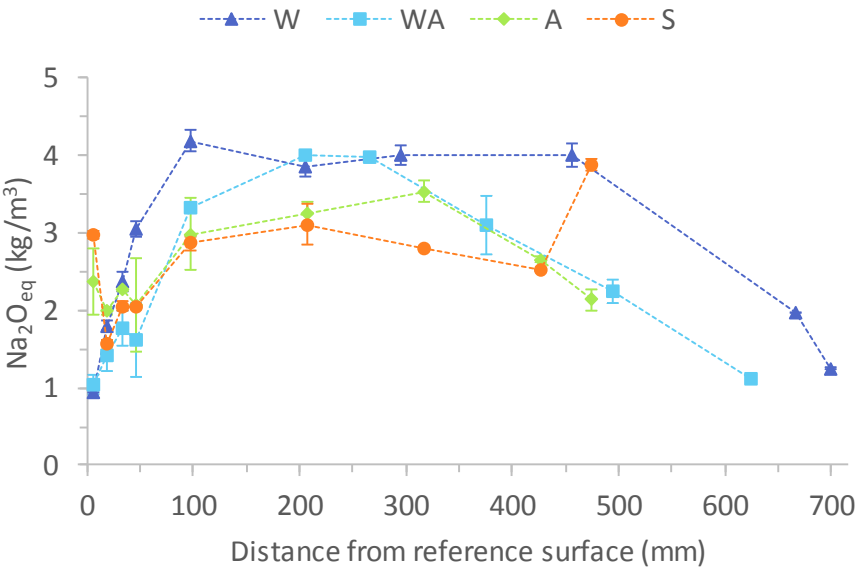

Figure 15: Comparison of the free alkali metal profiles obtained for each location of the Dam (W, WA, A, and S) from CWE. The data are expressed in kg/m³ Na_2O_{eq} and cover the full length of the cores. The results shown have not been corrected for the contribution of alkali from the aggregates during CWE.

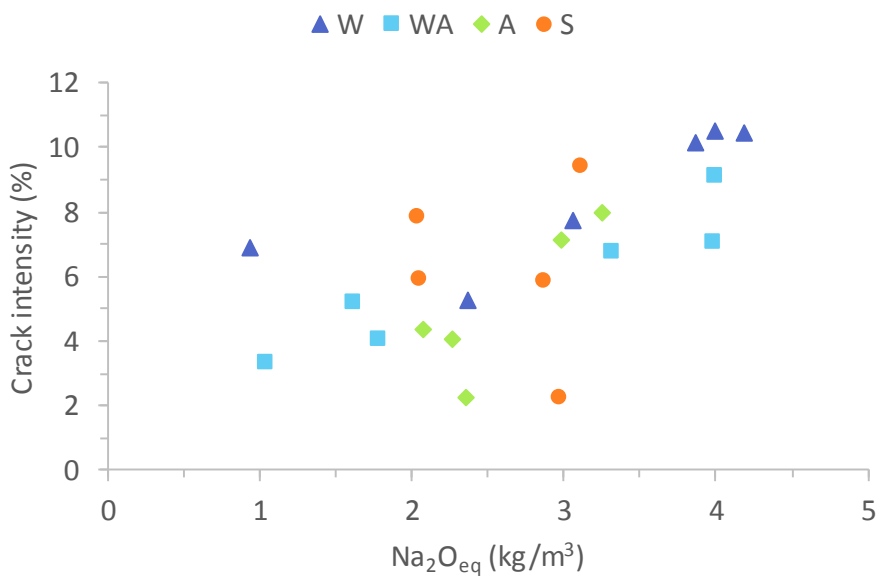

Figure 16: Crack intensity (%) in function of the alkali metal content (Na_2O_{eq}, kg/m³)

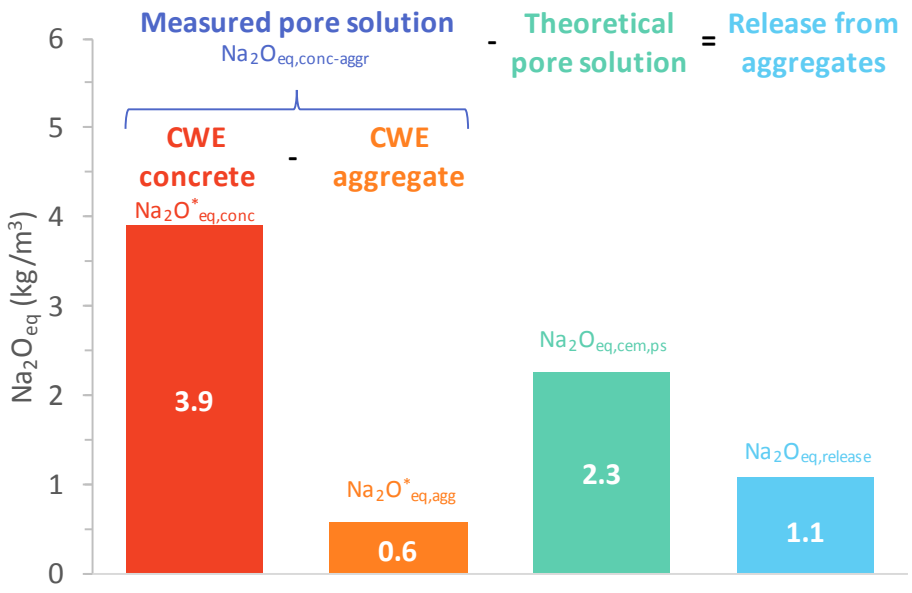

Figure 17: Calculation of the alkali metal release based on the CWE measurements obtained at location W, 200 mm from the reference surface, and considering $\%Na_2O_{eq}$ = 1.28% and k_{free} = 50%.

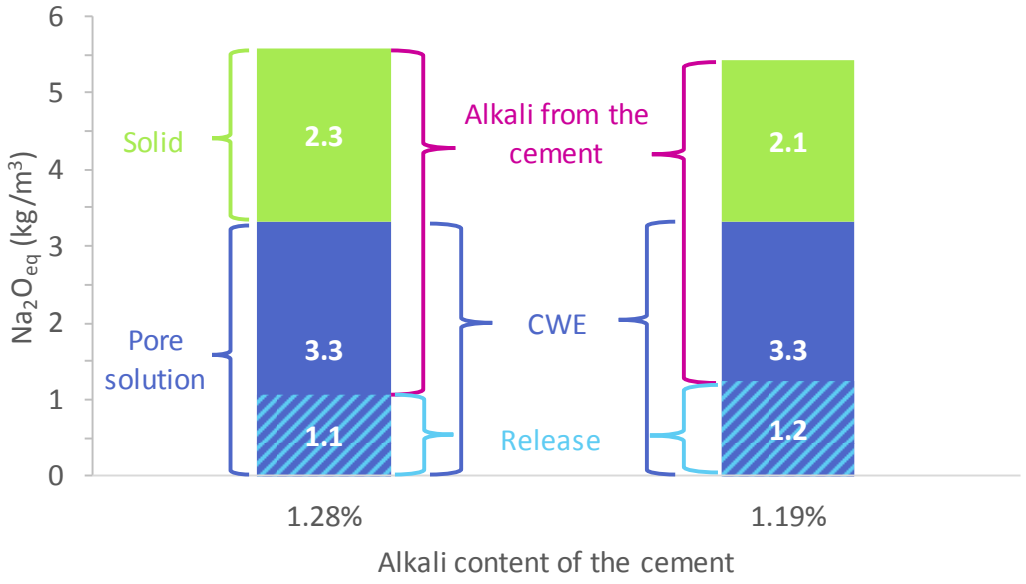

Figure 18: Alkali metals inventory of the concrete in the non-leached area of location W. Two cases are illustrated, one for each of the assumed alkali metal contents of the cement (1.28% and 1.19%). K_{free} is fixed at 50%.

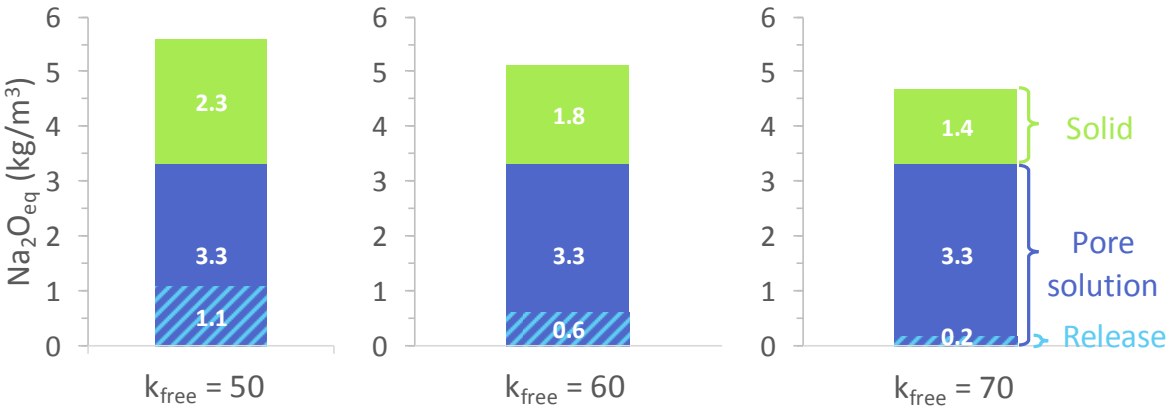

Figure 19: Impact of the assumed proportion of free alkali metals in the pore solution (k_{free}) on the alkali metal inventory. $\%Na_2O_{eq}$ is fixed at 1.28%.